Spin pumping from permalloy into uncompensated antiferromagnetic Co doped zinc oxide

View Online   Export Citation   CrossMark

Martin Buchner,[1] Julia Lumetzberger,[1] Verena Ney,[1] [ID] Taddäus Schaffers,[1,a)] [ID] Niéli Daffé,[2] [ID]
and Andreas Ney[1,b)] [ID]

AFFILIATIONS

[1]Institut für Halbleiter- und Festkörperphysik, Johannes Kepler Universität, Altenberger Str. 69, 4040 Linz, Austria
[2]Swiss Light Source, Paul Scherrer Institut, CH-5232 Villigen PSI, Switzerland

a)**Current address:** NanoSpin, Department of Applied Physics, Aalto University School of Science, P.O. Box 15100, FI-00076 Aalto, Finland.
b)**Author to whom correspondence should be addressed:** andreas.ney@jku.at. Phone/Fax: +43-732-2468-9642.

ABSTRACT

Heterostructures of Co-doped ZnO and Permalloy were investigated for their static and dynamic magnetic interactions. The highly Co-doped ZnO is paramagnetic at room temperature and becomes an uncompensated antiferromagnet at low temperatures, showing a narrowly opened hysteresis and a vertical exchange-bias shift even in the absence of any ferromagnetic layer. At low temperatures in combination with Permalloy, an exchange bias is found causing a horizontal as well as a vertical shift of the hysteresis of the hetero-structure together with an increase in coercive field. Furthermore, an increase in the Gilbert damping parameter at room temperature was found by multifrequency ferromagnetic resonance (FMR), indicating spin pumping. Temperature dependent FMR shows a maximum in magnetic damping close to the magnetic phase transition. These measurements also evidence the exchange-bias interaction of Permalloy and long-range ordered Co–O–Co structures in ZnO, which are barely detectable by SQUID due to the shorter probing times in FMR.

I. INTRODUCTION

In spintronics, a variety of concepts have been developed over the past few years to generate and manipulate spin currents.[1,2] Among them are the spin Hall effect (SHE), which originates from the spin–orbit coupling,[3] spin caloritronics,[4] utilizing the spin Seebeck effect,[5] or spin-transfer torque (current induced torque) due to angular momentum conservation[6] as examples. Spin pumping,[7] where a precessing magnetization transfers angular momentum to an adjacent layer, proved to be a very versatile method since it has been reported for different types of magnetic orders[8–11] or electrical properties[12–14] of materials. Furthermore, it could also be verified in trilayer systems where the precessing ferro-magnet and the spin sink, into which the angular momentum is transferred, are separated by a nonmagnetic spacer.[15–18] This is strongly dependent on the material, while for Cu,[15] Au,[16] or Al[17] pumping through a few nanometers is possible, an MgO barrier of 1 nm is enough to completely suppress spin pumping.[18]

Spintronic devices are usually based on a ferromagnet (FM), although antiferromagnetic spintronics[19] holds the advantages of faster dynamics, less perturbation by external magnetic fields, and no stray fields. The latter two are caused by the zero net mag-netization of an antiferromagnet (AFM), which on the other hand makes them harder to manipulate. One way to control an AFM is by using an adjacent FM layer and exploiting the exchange-bias (EB) effect.[20,21] Measuring spin-transfer torque in FM/AFM bilayer structures is possible[22,23] but challenging due to Joule heating[24–26] or possible unstable antiferromagnetic orders.[27] Antiferromagnets can be used either as spin source[28] or as spin sink[11,29] in a spin pumping experiment. As a result, the spin mixing conductance, a measure for the absorption of angular (spin) momentum at the interface,[7] is described by intersublattice scattering at an antiferro-magnetic interface.[30] The linear response theory predicted an enhancement of spin pumping near magnetic phase transitions,[31] which could recently also be verified experimentally.[29]

In this work, we investigate the behavior of the uncompensated, antiferromagnetic $Co_xZn_{1-x}O$ with $x \in \{0.3, 0.5, 0.6\}$ (in the following 30%, 50%, and 60% Co:ZnO) in contact with ferromagnetic Permalloy (Py). While weakly paramagnetic at room temperature, Co:ZnO makes a phase transition to an antiferromagnetic state at a Néel temperature (T_N) dependent on the Co concentration.[32] This resulting antiferromagnetism is not fully compensated, which is evidenced by a narrow hysteresis and a nonsaturating magnetization up to 17 T.[33] Furthermore, Co:ZnO films exhibit a vertical EB in complete absence of a FM layer.[34] This vertical exchange shift is dependent on the Co concentration,[32] temperature, and cooling field,[35] and the field imprinted magnetization predominantly shows orbital character.[36] Note that below the coalescence limit of 20%, the vertical EB vanishes. The uncompensated antiferromagnetism and its implications are strongly dependent on the Co concentration,[32,35] since the degree of antiferromagnetic compensation is increased for high Co concentrations. Therefore, Co:ZnO in contact with a FM layer gives the opportunity to study the coupling between FM and uncompensated AFM layers at different degrees of the antiferromagnetic compensation. Furthermore, the uncompensated moments in Co:ZnO are present due to the dopant configurations and are not a result of finite size or surface roughness effects.

Static coupling, visible as EB, is investigated using superconducting quantum interference device (SQUID) magnetometry. The dynamic coupling across the interface is measured using ferromagnetic resonance (FMR) at room temperature and around the magnetic transition temperatures determined from $M(T)$ SQUID measurements. Element selective x-ray magnetic circular dichroism (XMCD) studies are carried out to disentangle the individual magnetic contributions. Finally, heterostructures with an Al spacer were investigated to rule out intermixing at the interface as a source for the coupling effect.

II. EXPERIMENTAL DETAILS

Heterostructures consisting of Co:ZnO, Py, and Al, as shown in Fig. 1(a), were fabricated on c-plane sapphire substrates using reactive magnetron sputtering (RMS) and pulsed laser deposition (PLD) at a process pressure of 4×10^{-3} mbar. The different layers of a heterostructure are all grown in the same UHV chamber with a base pressure of 2×10^{-9} mbar in order to ensure an uncontaminated interface. While Py and Co:ZnO are grown by magnetron sputtering, the Al spacer and capping layers are grown by PLD. Al and Py are fabricated at room temperature using 10 standard cubic centimeters per minute (sccm) Ar as a process gas.

For the heterostructures containing a Co:ZnO layer, samples with three different Co concentrations of 30%, 50%, and 60% are grown utilizing preparation conditions that yield the best crystalline quality known for Co:ZnO single layers.[32,33,36] The Co concentration of films prepared according to these growth parameters has been checked with energy dispersive x-ray fluorescence and found to be the nominal one for 50% and 60% Co:ZnO. Nominally 30% Co:ZnO concentrations ranging between 30% and 35% Co have been determined. To sputter 30% and 50% Co:ZnO, metallic sputter targets of Co and Zn are used at an $Ar:O_2$ ratio of 10 : 1 sccm, while for 60% Co:ZnO, no oxygen and a ceramic composite target of ZnO and Co_3O_4 with a 3 : 2 ratio is used. The optimized growth
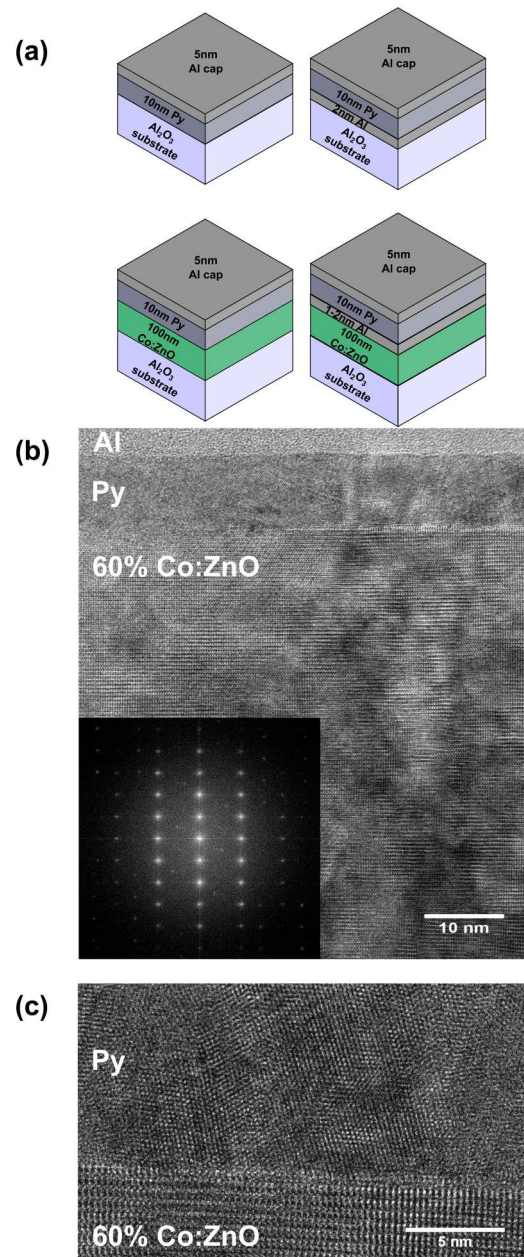

FIG. 1. (a) shows the schematic setup of the samples. For the Co:ZnO layer, three different Co concentrations of 30%, 50%, and 60% are used. The cross-sectional TEM image of the 60% Co:ZnO/Py sample as well as the electron diffraction pattern of the Co:ZnO layer (b) and a magnification on the interface between Co:ZnO and Py (c) are shown.

temperatures are 450 °C, 294 °C, and 525 °C. Between Co:ZnO growth and the next layer, a cool-down period is required to minimize interdiffusion between Py and Co:ZnO.

The static magnetic properties are investigated by SQUID magnetometry. $M(H)$ curves are recorded at 300 K and 2 K in

in-plane geometry with a maximum magnetic field of ± 5 T. During cooldown, either a magnetic field of ± 5 T or zero magnetic field is applied to differentiate between plus-field-cooled (pFC), minus-field-cooled (mFC), or zero-field-cooled (ZFC) measurements. All measurements shown in this work have been corrected by the diamagnetic background of the sapphire substrate, and care was taken to avoid well-known artifacts.[37,38]

For probing the element selective magnetic properties, x-ray absorption (XAS) measurements were conducted at the X-Treme beamline[39] at the Swiss Synchrotron Lightsource (SLS). From the XAS, the x-ray magnetic circular dichroism (XMCD) is obtained by taking the direct difference between XAS with left and right circular polarization. The measurements were conducted with a total fluorescence yield under 20° grazing incidence. As a result, the maximum magnetic field of 6.8 T was applied. Both external magnetic field and photon helicity have been reversed to minimize measurement artifacts. Again, pFC, mFC, and ZFC measurements were conducted applying either zero or the maximum field in the respective direction.

The dynamic magnetic properties were measured using multifrequency and temperature dependent FMR. Multifrequency FMR is exclusively measured at room temperature from 3 GHz to 10 GHz using a short circuited semirigid cable.[40] A nominal microwave power of 18 dBm ($\approx$63 mW) is used to excite the precession. This is far below a high frequency magnetic field amplitude of 3 mT (corresponding to 1 W of microwave power), and thus, the excitation power is below the Suhl instability region.[41] Temperature dependent measurements are conducted using an X-band resonator at 9.5 GHz. For these resonator based FMR, a microwave power of 0.2 mW is sufficient to excite the precession. Starting at 4 K, the temperature is increased to 50 K in order to be above the Néel temperature of the Co:ZnO samples.[32,35] At both FMR setups, the measurements were done in the in-plane direction. The magnetic field was applied in the easy direction determined at room temperature for all FMR measurements.

The measured raw data for SQUID, FMR, XAS, and XMCD can be found in the following data repository.[42]

III. EXPERIMENTAL RESULTS AND DISCUSSION

Figure 1(a) displays the four different types of samples: Co:ZnO layers, with Co concentrations of 30%, 50%, and 60%, are grown with a nominal thickness of 100 nm and Py with 10 nm. To prevent surface oxidation, a capping layer of 5 nm Al is used. For single 60% Co:ZnO films, the vertical exchange-bias effect was largest compared to lower Co concentrations. Therefore, 60% Co:ZnO samples with an additional Al layer as a spacer between Co:ZnO and Py have been fabricated. The thickness of the Al spacer (1 nm, 1.5 nm, and 2 nm) is in a range where the Al is reported not to suppress spin pumping effects itself.[17]

A. TEM

To get information about the interface between Py and Co:ZnO, high resolution cross-sectional transmission electron microscopy (TEM) was done. In Fig. 1(b), the cross section TEM image of 60% Co:ZnO/Py with the electron diffraction pattern of the Co:ZnO is shown. A magnification of the interface between

Co:ZnO and Py is shown in Fig. 1(c). From XRD measurements,[32] it is obvious that the quality of the wurtzite crystal slightly decreases for higher Co doping in ZnO. A similar behavior is observed in TEM cross section images. While 35% Co:ZnO shows the typical only slightly misoriented columnar grain growth,[32] it is obvious from Fig. 1(b) that the crystalline nanocolumns are less well ordered for 60% Co:ZnO. Although the electron diffraction pattern confirms a well ordered wurtzite structure, the misorientation of lattice plains is stronger than for 35% Co:ZnO,[32] even resulting in faint Moiré fringes, which stem from tilted lattice plains along the electron path. This corroborates previous findings of ω-rocking curves in XRD[32,36] where the increase in the full width at half maximum also evidences a higher tilting of the crystallites, i.e., an increased mosaicity. The interface to the Py layer is smooth, although it is not completely free of dislocations. Also, the interface seems to be rather abrupt within one atomic layer, i.e., free of intermixing. A similar behavior is found for the interface between 50% Co:ZnO and Py (not shown).

B. XAS and XMCD

Figure 2 shows XAS and XMCD spectra recorded at 3 K and a magnetic field of 6.8 T at the Ni $L_{3/2}$ and Co $L_{3/2}$ edges of 60% Co:ZnO/Py after pFC, mFC, or ZFC. For all three cooling conditions, the Ni $L_{3/2}$ edges [Fig. 2(a)] show a metallic character of the
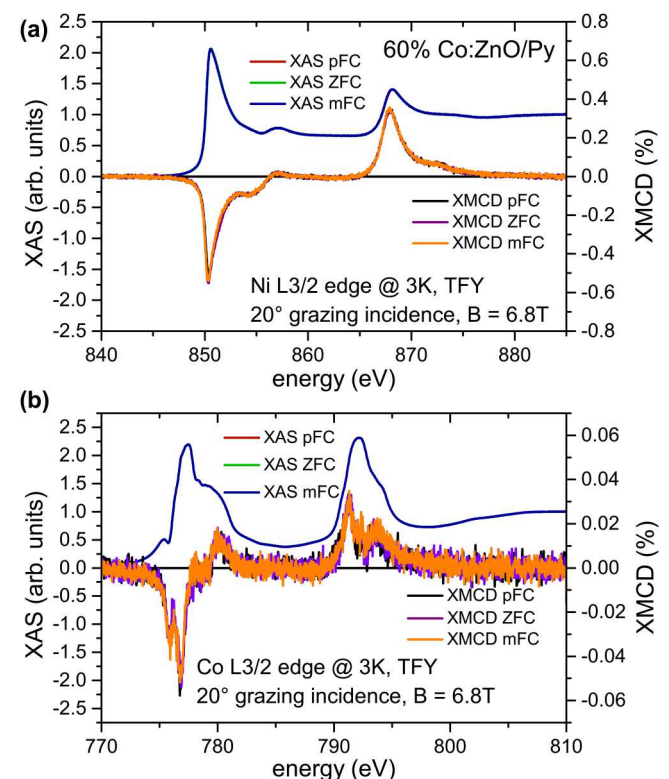

FIG. 2. In (a), the XMCD at the Ni $L_{3/2}$ edges after pFC, mFC, and ZFC for 60% Co:ZnO/Py are shown. (b) shows the same for the Co $L_{3/2}$ edges.

Ni XAS without any additional fine structure characteristics for NiO and thus no sign of oxidation of the Py. Furthermore, no differences in the XAS or the XMCD of the Ni edges of different cooling conditions are found. The same is observed for the Fe $L_{3/2}$ edges; however, they are affected greatly by self-absorption processes in a total fluorescence yield (not shown).

The Co $L_{3/2}$ edges in Fig. 2(b) are also greatly affected by the self absorption of the total fluorescence yield, since it is buried below 10 nm of Py and 5 nm of Al. In contrast to Ni, the XAS and XMCD at the Co $L_{3/2}$ edges [Fig. 2(b)] are not metallic and evidence the incorporation of Co as Co^{2+} in the wurtzite structure of ZnO.[32,36] The overall intensity of the Co XMCD is strongly reduced, indicating a small magnetic moment per Co atom well below metallic Co. This small effective Co moment in 60% Co:ZnO can be understood by the degree of antiferromagnetic compensation that increases with higher Co doping concentrations.[32] Furthermore, no indications of metallic Co precipitates are visible in the XAS and XMCD of the heterostructure as it would be expected for a strong intermixing at the interface to the Py.

No changes between the pFC, mFC, and ZFC measurements are visible also for the Co edges either in XAS or XMCD, indicating that the spin system of the Co dopants is not altered in the exchange-bias state. This corroborates measurements conducted at the Co K-edge.[36] After field cooling, the XMCD at the Co main absorption increased compared to the ZFC conditions. At the Co K-edge, the main absorption stems from the orbital moment. The spin system is only measured indirectly at the pre-edge feature, which remained unaffected by the cooling field conditions. The data of K- and L-edges combined evidence that the imprinted magnetization after field cooling is composed predominantly of the orbital moment, which is in good agreement with other EB systems.[43,44]

C. SQUID

The static coupling in the heterostructures was investigated by integral SQUID magnetometry. Measurements done at 300 K, as shown in Fig. 3(a), do not reveal a significant influence of the Co:ZnO on the $M(H)$ curve of Py. Just a slight increase in the coercive field from 0.1 mT to 0.4 mT is determined. Some of the $M(H)$ curves in Fig. 3(a) are more rounded than the others. This can be attributed to slight variations in the aspect ratio of the SQUID pieces and thus variations in the shape anisotropy. The inset of Fig. 3(a) shows the hysteresis of the single Py film at 300 K and 2 K, where no difference in coercivity is visible. Please note that up to now, measurements were conducted only in a field range of ± 10 mT and directly after a magnet reset. This is done to avoid influences of the offset field of the SQUID.[38] At low temperatures, to determine the full influence of Co:ZnO, high fields need to be applied, as it has been shown in Ref. 35. Therefore, coercive fields obtained from low temperature measurements are corrected by the known offset field of 1.5 mT of the SQUID.[38]

Since the paramagnetic signal of Co:ZnO is close to the detection limit of the SQUID and thus orders of magnitude lower than the Py signal, it has no influence on the room temperature $M(H)$ curve. However, with an additional Co:ZnO layer, a broadening of the hysteresis and a horizontal and a small vertical shift are measured at 2 K as can be seen exemplarily for 60% Co:ZnO/Py in Fig. 3(b).
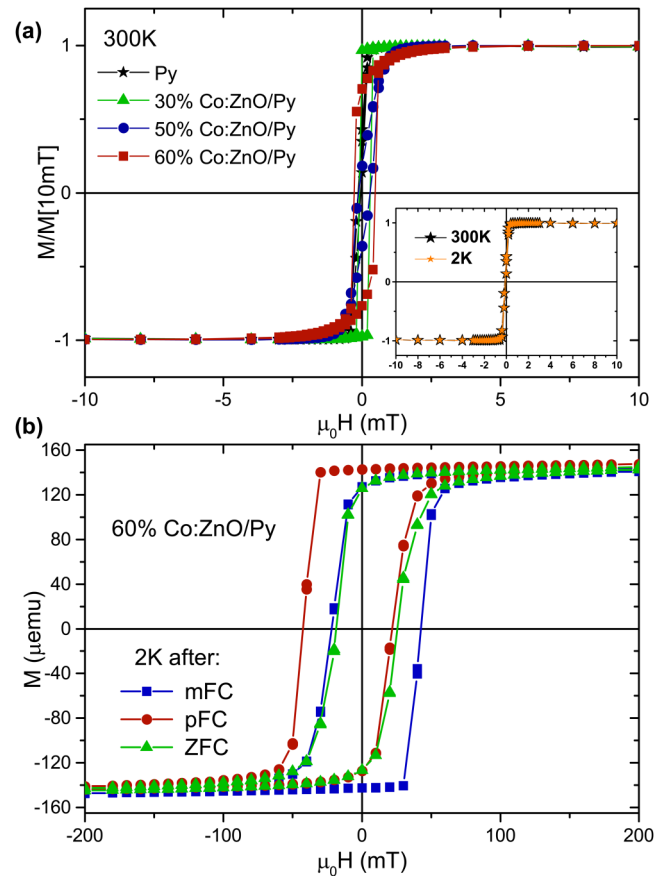

FIG. 3. At 300 K, the $M(H)$ curves of the single Py film almost overlap with the $M(H)$ curves of the heterostructures with all three Co:ZnO concentrations (a). In the inset, it can be seen that there is no difference in the coercive field for Py at 300 K and 2 K. Measuring the 60% Co:ZnO/Py heterostructure after plus, minus, and zero-field cooling, horizontal and vertical exchange-bias shifts are visible, as well as an increase in the coercive field (b).

Similar to single Co:ZnO films where an opening of the $M(H)$ curve is already visible in ZFC measurements[32,34–36] also in the heterostructure, no field cooling is needed to increase the coercive field.

Earlier works[32,34] demonstrated that the hysteresis opening and vertical shift in Co:ZnO are strongly dependent on the Co concentration and increase with increasing Co doping level. Furthermore, the EB effects are observed in the in-plane and out-of-plane direction, with a greater vertical shift in the plane. Therefore, the heterostructures with Py are measured with the magnetic field in the in-plane direction. Figure 4(a) provides an overview of the coercive field after ZFC for the different Co concentrations. The coercive field increases from 0.1 mT for single Py to 20.6 mT for 60% Co:ZnO/Py. Additionally, in the inset, the temperature dependence of the coercive field of the 60% Co:ZnO/Py heterostructure is shown, since it shows the strongest increase in the coercive field. From the 20.6 mT at 2 K, it first increases slightly when warming up to 5 K. That the maximum coercivity is not at 2 K is in good agreement with
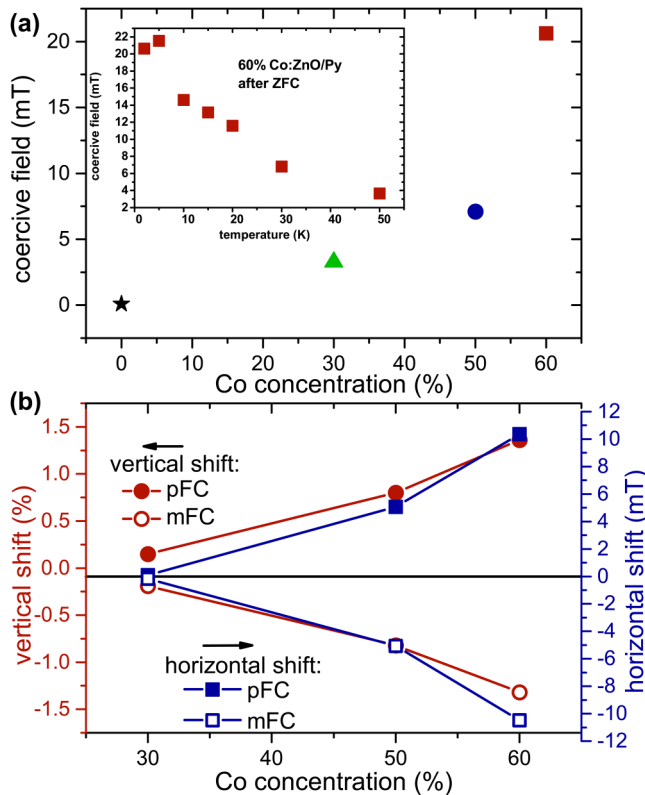
FIG. 4. (a) At 2 K, the coercivity increases with Co concentration in the heterostructure. In the inset, the temperature dependence of the coercivity of the 60% Co:ZnO/Py heterostructure is given. (b) The vertical shift (circles) and the horizontal shift (squares) depend on the Co concentration. Both shifts reverse the direction when the measurement is changed from pFC to mFC.

measurements at single 60% Co:ZnO films where a maximum hysteresis opening at 7 K was determined.[35] Afterward, the coercive field decreases. At the Néel temperature of 20 K, a coercive field of 11.6 mT is measured. Above T_N, it decreases even further, but the coercivity is still 3.65 mT at 50 K. A coupling above T_N could stem from long-range magnetic ordered structures in Co:ZnO where first indications are visible already in single Co:ZnO films.[32] However, for single layers, they are barely detectable with the SQUID.

The vertical (circles) and horizontal (squares) hysteresis shifts after pFC and mFC are shown in Fig. 4(b) for the Py samples with Co:ZnO layers. Similar to single Co:ZnO films, the vertical shift increases with rising Co concentration. The shift is given in percent of the magnetization at 5 T to compensate for different sample sizes. Due to the higher overall magnetization at 5 T in combination with Py, this percentage for the heterostructures is lower than the vertical shift for single Co:ZnO films. This is an indication that the vertical shift stems solely from the Co:ZnO layer, and no additional component due to the coupling with the Py layer appears, which is in good agreement with Ref. 36. With increasing Co concentration, the degree of antiferromagnetic compensation increases,[32,35] which in

turn should lead to a stronger EB coupling. This can be seen in the horizontal shift and thus the EB field, which is strongest for 60% Co:ZnO/Py and nearly gone for 30% Co:ZnO/Py. For both kinds of shift, the pFC and mFC measurements behave similarly, except the change in the direction of the shifts.

D. Multifrequency FMR

The dynamic coupling between the two layers has been investigated by multifrequency FMR measured at room temperature. The frequency dependence of the resonance position between 3 GHz and 10 GHz of the heterostructures is shown in Fig. 5(a). The resonance position of Py yields no change regardless of the Co concentration in the Co:ZnO layer or its complete absence. Also, in 2 nm Al/Py and 60% Co:ZnO/2 nm Al/Py, the resonance position
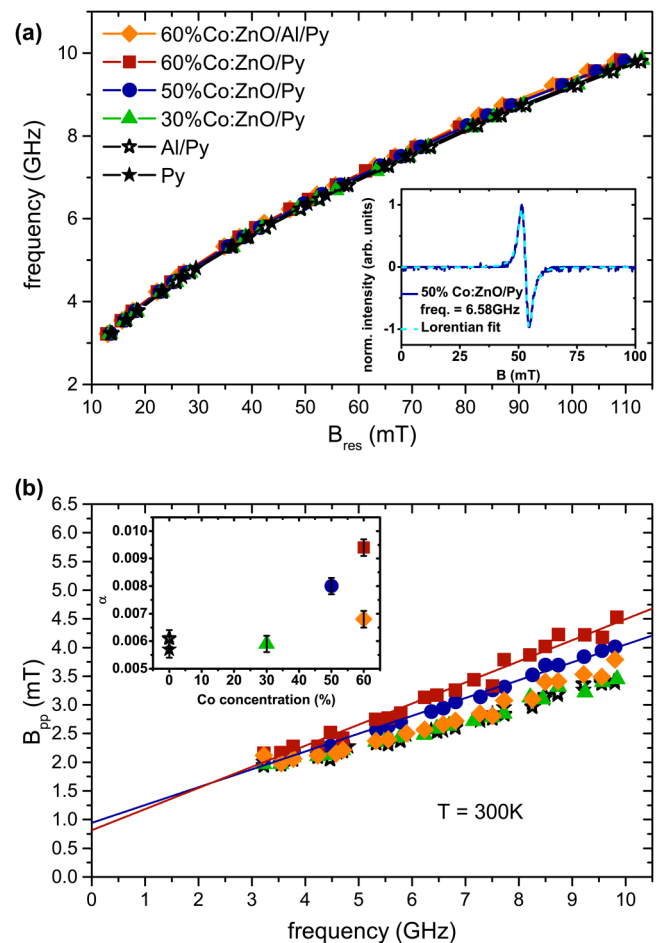

FIG. 5. The resonance fields determined at room temperature with multifrequency FMR are seen in (a). In the inset, an exemplary FMR spectrum of 50% Co:ZnO/Py at 6.58 GHz is shown with the corresponding Lorentzian fit. For the linewidth (b) and the associated damping parameter α (inset), an increase is visible for the heterostructures with a higher Co concentration in the Co:ZnO. The lines are linear fits to the data.

stays unchanged. The resonance position of a thin film is given by the Kittel formula,[45]

$$f = \frac{\gamma}{2\pi}\sqrt{B_{res}(B_{res} + \mu_0 M)}, \tag{1}$$

with the gyromagnetic ratio $\gamma = \frac{g\mu_B}{\hbar}$ and magnetization M. However, any additional anisotropy adds to B_{res} and, therefore, alters Eq. (1).[45] The fact that all samples show the identical frequency dependence of the resonance position evidences that neither the gyromagnetic ratio γ and thus the Py g-factor are influenced nor any additional anisotropy B_{Aniso} is introduced by the Co:ZnO. By fitting the frequency dependence of the resonance position using the Kittel equation with the g-factor of 2.11,[46] all the samples are in the range of (700 ± 15) kA/m, which within error bars is in good agreement with the saturation magnetization of (670 ± 50) kA/m determined from SQUID.

No difference in linewidth between Al/Py (open stars) and Py (full stars) is found, as can be seen in Fig. 4(b) where the peak to peak linewidth B_{pp} is plotted over the measured frequency range for all the heterostructures. While the heterostructure with 30% Co:ZnO/Py (green triangles) lies atop the single Py and the Al/Py film, the linewidth increases stronger with frequency for 50% Co:ZnO/Py (blue circles). The broadest FMR lines are measured for the 60% Co:ZnO/Py heterostructure (red squares). Therefore, the Co:ZnO layers do not influence the resonance position of the FMR measurement, but the heterostructures exhibit an increased linewidth, which in general contains the following contributions:

$$\Delta B = \Delta B_{hom} + \Delta B_{2M} + \Delta B_{mosaic} + \Delta B_{inhom}, \tag{2}$$

which can be separated by their frequency dependence. Homogeneous (Gilbert-like) contributions ΔB_{hom} due to an increased damping show a linear behavior in the frequency,

$$\Delta B_{hom} = \frac{4\pi\alpha}{\gamma}f, \tag{3}$$

from which the Gilbert damping parameter α can be determined. Broadening due to two magnon scattering ΔB_{2M}[47,48] and due to mosaicity ΔB_{mosaic}[49,50] exhibits a nonlinear frequency dependence, while inhomogeneous contributions ΔB_{inhom} do not depend on frequency and, therefore, give the y axis intersect. Two magnon scattering is easily mistaken for linear behavior at low frequencies and, therefore, sometimes mistaken for Gilbert-like contributions. However, up to 10 GHz, no indications of nonlinear frequency behavior are apparent, and thus, we consider the contributions from ΔB_{2M} and ΔB_{mosaic} to be negligible so that the broadening is dominated by homogeneous, i.e., Gilbert-like damping.

Using the Py g-factor of 2.11,[46] α can be calculated from the slopes of the frequency dependence extracted from the linewidths seen in Fig. 5(b): the resulting α is shown in the inset. For the single Py layer, $\alpha_{Py} = (5.7 \pm 0.3) \times 10^{-3}$, which compares well to previously reported values.[7] This increases to $\alpha_{50} = (8.0 \pm 0.3) \times 10^{-3}$ for 50% Co:ZnO/Py and even $\alpha_{60} = (9.4 \pm 0.3) \times 10^{-3}$ for 60% Co:ZnO/Py. Therefore, the damping increases by a factor of 1.64, resulting in a $\Delta\alpha = \alpha_{60} - \alpha_{Py} = (3.7 \pm 0.5) \times 10^{-3}$, indicating angular momentum transfer and thus spin pumping from the Py

into the Co:ZnO layer. By insertion of a 2 nm Al spacer layer, $\Delta\alpha$ reduces to $(0.8 \pm 0.5) \times 10^{-3}$.

E. Dependence on the Al spacer thickness

To obtain information about the lengthscale of the static and dynamic coupling, heterostructures with Al spacer layers of different thicknesses (1 nm, 1.5 nm, and 2 nm thick) between Py and the material beneath (sapphire substrate or 60% Co:ZnO) were fabricated. Without a Co:ZnO layer, the spacer underlying the Py layer does not exhibit any changes in either SQUID (not shown) or FMR [see Figs. 5(a) and 5(b)]. The results obtained for the 60% Co:ZnO/Al/Py heterostructure for the coercive field, vertical and horizontal shift extracted from $M(H)$ curves measured at 2 K, are shown in Fig. 6(a), whereas the damping parameter α from room temperature multifrequency FMR measurements, an analog to Fig. 5(b), is depicted in Fig. 6(b).

The horizontal shift and increased coercive field are caused by the coupling of FM and AFM moments in a range of a few angstroms to the interface.[51–53] Therefore, both effects show a similar decrease by the insertion of an Al spacer. While the horizontal shift
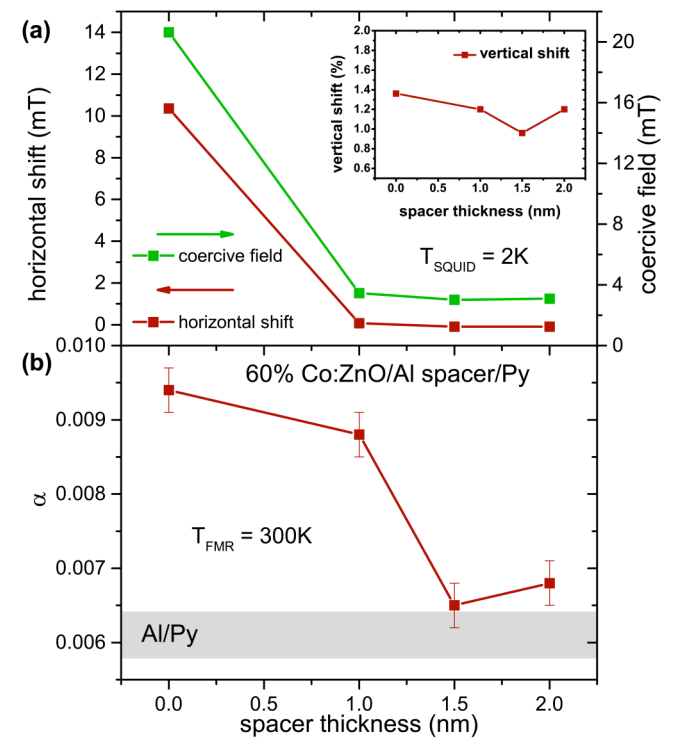

FIG. 6. When an Al spacer is inserted between the Py and Co:ZnO layer, the horizontal shift and coercive field shows a strong decrease already at 1 nm spacer thickness (a), while the vertical shift (inset) is not dependent on the spacer thickness. (b) shows the effect of the Al spacer on the Gilbert damping parameter α, which also decreases if the spacer gets thicker than 1 nm. As shaded region, the Gilbert damping parameter of a Al/Py film is indicated within error bars.

and coercive field are reduced significantly already at a spacer thickness of 1 nm, the vertical shift [the inset of Fig. 6(a)] is nearly independent of the Al spacer. Comparing with the XMCD spectra of Fig. 2, it can be concluded that the vertical shift in the uncompensated AFM/FM system Co:ZnO/Py stems solely from the increased orbital moment of pinned uncompensated moments in Co:ZnO and is independent of the FM moments at the interface. Furthermore, the FM moments do not exhibit any vertical shift, and the exchange between the two layers only results in the horizontal shift.

For the room temperature FMR measurements after inserting an Al spacer, no effect on the resonance position is found, as was shown already in Fig. 5(a). For a 1 nm thick Al spacer, the damping results in $\alpha = (8.8 \pm 0.3) \times 10^{-3}$, which gives a $\Delta\alpha = (3.1 \pm 0.5) \times 10^{-3}$. This is only a slight decrease compared to the sample without an Al spacer. By increasing the spacer thickness, α reduces to values just above the damping obtained for pure Py or Al/Py, shown as a shaded region in Fig. 6(b). In principle, the spin diffusion length of Al is larger than 1.5 nm, and spin pumping should still be visible. However, the additional interfaces

may influence the damping. The interface between Py and Al can be excluded since the Al/Py heterostructure shows no change compared to single Py films, indicating a stronger influence from the Co:ZnO/Al interface. However, the 1 nm thick Al layer is thick enough to suppress intermixing between the Co:ZnO and Py layer as can be seen in Fig. 1(b), which in turn can be ruled out as a source of the increased damping. This indicates further that the increased damping stems from a dynamic coupling effect like spin pumping from Py into Co:ZnO. Furthermore, the dynamic coupling mechanism extends over a longer range than the static coupling. With a 1 nm spacer, the dynamic coupling is only slightly reduced, whereas the static coupling is already completely suppressed.

F. Temperature dependent FMR

In the vicinity of the magnetic phase transition temperature, the spin pumping efficiency should be at a maximum.[29,31] Therefore, the samples are measured inside a resonator based FMR setup, as a function of temperature. During the cooldown, no magnetic field is applied, and the results shown in Fig. 7 are ZFC measurements.
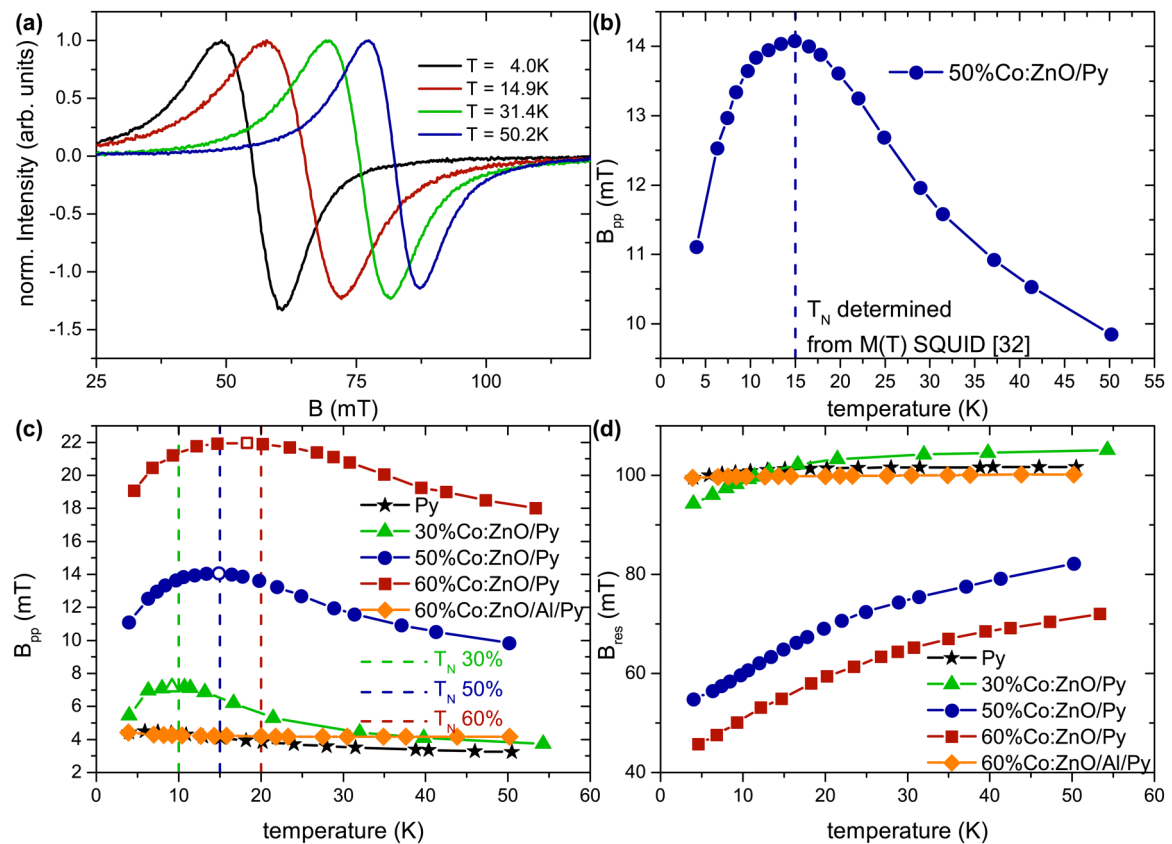

FIG. 7. By decreasing the temperature, the resonance position of 50% Co:ZnO/Py shifts to lower resonance fields (a) and the linewidth increases, showing a maximum at the T_N (b). A similar behavior is observed for the heterostructures with 30% and 60% Co doping, while a single Py film does not exhibit a maximum when cooling (c). The maximum is marked as an open symbol in the temperature dependence, while the T_N determined from $M(T)$[32] are shown as dashed lines. Furthermore, the resonance position of the heterostructures with Co:ZnO shifts at low temperatures (d).

For 50% Co:ZnO/Py, the resonance position of Py shifts to lower magnetic fields with decreasing temperature, as can be seen in Fig. 7(a). Not only the resonance position is shifting, but also the linewidth is changing with temperature as shown in Fig. 7(b). The linewidth has a maximum at a temperature of 15 K, which corresponds well to T_N determined by $M(T)$ SQUID measurements for a 50% Co:ZnO layer.[32] This maximum of the linewidth in the vicinity of T_N is also observed for 60% Co:ZnO/Py and even 30% Co:ZnO/Py, as shown in Fig. 7(c), and is in good agreement with predictions of the linear response theory showing an increased spin pumping efficiency around the magnetic phase transition.[31] The measured maximum of 30% Co:ZnO/Py and 60% Co:ZnO/Py are at 10.7 K and 19.7 K, respectively, and are marked with an open symbol in Fig. 7(c). For comparison, the Néel temperatures determined from $M(T)$ measurements[32] are plotted as a dashed line. Py on the other hand shows only a slight increase in the linewidth with decreasing temperature. The observed effects at low temperatures vanish for the 60% Co:ZnO/2 nm Al/Py heterostructure.

Figure 7(d) shows the temperature dependence of the resonance field for all samples. For Py, B_{res} only decreases slightly, whereas for 50% and 60% Co:ZnO, a strong shift of B_{res} can be observed. This shift evidences a magnetic coupling between the Py and Co:ZnO layer. Even in the heterostructure with 30% Co:ZnO/Py, a clear decrease in the resonance position below 10 K (the previously determined T_N[32]) is visible. This shift of the resonance position is only observed at low temperatures. At room temperature, no shift of the resonance position at 9.5 GHz has been observed as shown in Fig. 5(a). From the low-temperature behavior of the single Py layer and Eq. (1), it is obvious that the gyromagnetic ratio is not changing strongly with temperature; therefore, the shift of the resonance position in the heterostructure can be attributed to a change in anisotropy. From the SQUID measurements at 2 K, see Figs. 3(b) and 4(b), EB between the two layers has been determined, which acts as additional anisotropy[20] and, therefore, causes the shift of the resonance position. Both the shift of the resonance position and the maximum in the FMR linewidth vanish if the Py is separated from 60% Co:ZnO by a 2 nm Al spacer layer. Therefore, also at low temperatures, the static EB coupling and dynamic coupling can be suppressed by an Al spacer layer.

$M(T)$ measurements indicated a more robust long-range magnetic order in 60% Co:ZnO by a weak separation of the field heated and ZFC curves lasting up to 200 K.[32] Additionally, the coercive field measurements on the 60% Co:ZnO/Py heterostructure revealed a weak coupling above T_N. However, this has not been observed for lower Co concentrations. In the heterostructure with 30% Co:ZnO, the FMR resonance position and linewidth return quickly to the room temperature value for temperatures above the T_N of 10 K. For both 50% Co:ZnO/Py and 60% Co:ZnO/Py, the resonance positions are still decreased and the linewidths are increased above their respective Néel temperatures and are only slowly approaching the room temperature value. In the 60% Co:ZnO/Py, heterostructure measurements between 100 K and 200 K revealed that a reduced EB is still present. It is known for the blocking temperatures of superparamagnetic structures that in FMR, a higher blocking temperature compared to SQUID is obtained due to much shorter probing times in FMR of the order of nanoseconds compared to seconds in SQUID.[54] Hence, large dopant configurations in Co:ZnO still appear to be blocked on time scales of the FMR, whereas they already appear unblocked on time scales of the SQUID measurements.

IV. CONCLUSION

The static and dynamic magnetic coupling of Co:ZnO, which is weakly paramagnetic at room temperature and an uncompensated AFM at low temperatures, with ferromagnetic Py was investigated by means of SQUID magnetometry and FMR. At room temperature, no static interaction is observed in the $M(H)$ curves. After cooling to 2 K, an EB between the two layers is found, resulting in an increase in the coercive field and a horizontal shift. Additionally, a vertical shift is present caused by the uncompensated moments in the Co:ZnO. While this vertical shift is nearly unaffected by the insertion of an Al spacer layer between Co:ZnO and Py, the EB vanishes already at a spacer thickness of 1 nm.

The FMR measurements at room temperature reveal an increase in the Gilbert damping parameter for 50% Co:ZnO/Py and 60% Co:ZnO/Py, whereas 30% Co:ZnO/Py is in the range of an individual Py film. At room temperature, the resonance position is not affected for all the heterostructures. For the 60% Co-doped sample, $\Delta\alpha = 3.7 \times 10^{-3}$, which is equivalent to an increase by a factor of 1.64, indicating spin pumping from Py into the Co:ZnO. In contrast to the static magnetic coupling effects, an increased linewidth is still observed in the heterostructure containing a 1 nm Al spacer layer.

At lower temperatures the resonance position of the heterostructures shifts to lower resonance fields, due to the additional EB anisotropy. The temperature dependence of the linewidth shows a maximum at temperatures, which by comparison with $M(T)$ measurements corresponds well to T_N of single Co:ZnO layers and thus corroborate the increase in the damping parameter, and thus, the dynamic coupling increases in vicinity to the magnetic phase transition. This is another indication for spin pumping from Py into Co:ZnO since it was predicted by the linear response theory that the spin pumping efficiency increases in vicinity to the antiferromagnetic phase transition. Furthermore, the shift of the resonance position has been observed at temperatures well above T_N for 50% Co:ZnO/Py and 60% Co:ZnO/Py. Up to now, only indications for a long-range AFM order in 60% Co:ZnO/Py had been found by static $M(T)$ measurements. The dynamic coupling, however, is sensitive to those interactions due to the higher time resolution in FMR, resulting in a shift in the resonance position above the T_N determined from $M(T)$ SQUID.

REFERENCES

[1] I. Žutić, J. Fabian, and S. Das Sarma, Rev. Mod. Phys. **76**, 323 (2004).

[2] J. Sinova and I. Žutić, Nat. Mater. **11**, 368 (2012).

[3] M. I. Dyakonov and V. I. Perel, JETP Lett. **13**, 467 (1971).

[4] G. E. W. Bauer, E. Saitoh, and B. J. van Wees, Nat. Mater. **11**, 391 (2012).

[5] K. Uchida, S. Takahashi, K. Harii, J. Ieda, W. Koshibae, K. Ando, S. Maekawa, and E. Saitoh, Nature **455**, 778 (2008).

[6] A. Brataas, A. D. Kent, and H. Ohno, Nat. Mater. **11**, 372 (2012).

[7] Y. Tserkovnyak, A. Brataas, and G. E. W. Bauer, Phys. Rev. Lett. **88**, 117601 (2002).

[8] S. Mizukami, Y. Ando, and T. Miyazaki, Jpn. J. Appl. Phys. **40**, 580 (2001).

[9] T. Taniguchi, S. Yakata, H. Imamura, and Y. Ando, Appl. Phys. Express **1**, 031302 (2008).

[10] R. Iguchi, K. Ando, E. Saitoh, and T. Sato, J. Phys.: Conf. Ser. **266**, 012089 (2011).

[11] P. Merodio, A. Ghosh, C. Lemonias, E. Gautier, U. Ebels, M. Chshiev, H. B. V. Baltz, and W. E. Bailey, Appl. Phys. Lett. **104**, 032406 (2014).

[12] K. Ando, S. Takahashi, J. Ieda, H. Kurebayashi, T. Trypiniotis, C. H. W. Barnes, S. Maekawa, and E. Saitoh, Nat. Mater. **10**, 655 (2011).

[13] W. Zhang, M. B. Jungfleisch, W. Jiang, J. E. Pearson, A. Hoffmann, F. Freimuth, and Y. Mokrousov, Phys. Rev. Lett. **113**, 196602 (2014).

[14] C. Hahn, G. de Loubens, V. V. Naletov, J. Ben Youssef, O. Klein, and M. Viret, Europhys. Lett. **108**, 57005 (2014).

[15] K. Lenz, T. Toliński, J. Lindner, E. Kosubek, and K. Baberschke, Phys. Rev. B **69**, 144422 (2004).

[16] E. Montoya, B. Kardasz, C. Burrowes, W. Huttema, E. Girt, and B. Heinrich, J. Appl. Phys. **111**, 07C512 (2012).

[17] Y. Kitamura, E. Shikoh, Y. Ando, T. Shinjo, and M. Shiraishi, Sci. Rep. **3**, 1739 (2013).

[18] A. A. Baker, A. I. Figueroa, D. Pingstone, V. K. Lazarov, G. van der Laan, and T. Hesjedal, Sci. Rep. **6**, 35582 (2016).

[19] V. Baltz, A. Manchon, M. Tsoi, T. Moriyama, T. Ono, and Y. Tserkovnyak, Rev. Mod. Phys. **90**, 015005 (2018).

[20] W. P. Meiklejohn and C. P. Bean, Phys. Rev. **102**, 1413 (1956).

[21] J. Nogués and I. K. Schuller, J. Magn. Magn. Mater. **192**, 203 (1999).

[22] Z. Wei, A. Sharma, A. S. Nunez, P. M. Haney, R. A. Duine, J. Bass, A. H. MacDonald, and M. Tsoi, Phys. Rev. Lett. **98**, 116603 (2007).

[23] Z. Wei, J. Basset, A. Sharma, J. Bass, and M. Tsoi, J. Appl. Phys. **105**, 07D108 (2009).

[24] X.-L. Tang, H.-W. Zhanga, H. Su, Z.-Y. Zhong, and Y.-L. Jing, Appl. Phys. Lett. **91**, 122504 (2007).

[25] N. V. Dai, N. C. Thuan, L. V. Hong, N. X. Phuc, Y. P. Lee, S. A. Wolf, and D. N. H. Nam, Phys. Rev. B **77**, 132406 (2008).

[26] X. L. Tang, H. W. Zhang, H. Su, Y. L. Jing, and Z. Y. Zhong, Phys. Rev. B **81**, 052401 (2010).

[27] S. Urazhdin and N. Anthony, Phys. Rev. Lett. **99**, 046602 (2007).

[28] S. Takei, B. I. Halperin, A. Yacoby, and Y. Tserkovnyak, Phys. Rev. B **90**, 094408 (2014).

[29] L. Frangou, S. Oyarzún, S. Auffret, L. Vila, S. Gambarelli, and V. Baltz, Phys. Rev. Lett. **116**, 077203 (2016).

[30] P. M. Haney and A. H. MacDonald, Phys. Rev. Lett. **100**, 196801 (2008).

[31] Y. Ohnuma, H. Adachi, E. Saitoh, and S. Maekawa, Phys. Rev. B **89**, 174417 (2014).

[32] V. Ney, B. Henne, J. Lumetzberger, F. Wilhelm, K. Ollefs, A. Rogalev, A. Kovacs, M. Kieschnick, and A. Ney, Phys. Rev. B **94**, 224405 (2016).

[33] B. Henne, V. Ney, K. Ollefs, F. Wilhelm, A. Rogalev, and A. Ney, Sci. Rep. **5**, 16863 (2015).

[34] B. Henne, V. Ney, M. de Souza, and A. Ney, Phys. Rev. B **93**, 144406 (2016).

[35] M. Buchner, B. Henne, V. Ney, and A. Ney, Phys. Rev. B **99**, 064409 (2019).

[36] M. Buchner, B. Henne, V. Ney, J. Lumetzberger, F. Wilhelm, A. Rogalev, A. Hen, and A. Ney, J. Appl. Phys. **123**, 203905 (2018).

[37] M. Sawicki, W. Stefanowicz, and A. Ney, Semicond. Sci. Technol. **26**, 064006 (2011).

[38] M. Buchner, K. Höfler, B. Henne, V. Ney, and A. Ney, J. Appl. Phys. **124**, 161101 (2018).

[39] C. Piamonteze, U. Flechsig, S. Rusponi, J. Dreiser, J. Heidler, M. Schmidt, R. Wetter, M. Calvi, T. Schmidt, H. Pruchova, J. Krempasky, C. Quitmann, H. Brune, and F. Nolting, J. Synchrotron Rad. **19**, 661–674 (2012).

[40] F. M. Römer, M. Möller, K. Wagner, L. Gathmann, R. Narkowicz, H. Zähres, B. R. Salles, P. Torelli, R. Meckenstock, J. Lindner, and M. Farle, Appl. Phys. Lett. **100**, 092402 (2012).

[41] T. Gerrits, P. Krivosik, M. L. Schneider, C. E. Patton, and T. J. Silva, Phys. Rev. Lett. **98**, 207602 (2007).

[42] Data repository for Johannes Kepler University Linz (Magnetic Oxides Group) at http://doi.org/10.17616/R3C78N; (preliminary) search tag: BLN19.

[43] D. Schmitz, E. Schierle, N. Darowski, H. Maletta, E. Weschke, and M. Gruyters, Phys. Rev. B **81**, 224422 (2010).

[44] P. Audehm, M. Schmidt, S. Brück, T. Tietze, J. Gräfe, S. Macke, G. Schütz, and E. Goering, Sci. Rep. **6**, 25517 (2016).

[45] C. Kittel, Phys. Rev. **73**, 155 (1948).

[46] S. Mizukami, Y. Ando, and T. Miyazaki, Phys. Rev. B **66**, 104413 (2002).

[47] J. Lindner, K. Lenz, E. Kosubek, K. Baberschke, D. Spoddig, R. Meckenstock, J. Pelzl, Z. Frait, and D. L. Mills, Phys. Rev. B **68**, 060102(R) (2003).

[48] K. Baberschke, J. Phys.: Conf. Ser. **324**, 012011 (2011).

[49] R. L. Rodríguez-Suárez, L. H. Vilela-Leão, T. Bueno, A. B. Oliveira, J. R. L. de Almeida, P. Landeros, S. M. Rezende, and A. Azevedo, Phys. Rev. B **83**, 224418 (2011).

[50] R. L. Rodríguez-Suárez, L. H. Vilela-Leão, T. Bueno, J. B. S. Mendes, P. Landeros, S. M. Rezende, and A. Azevedo, Appl. Phys. Lett. **100**, 242406 (2012).

[51] M. R. Fitzsimmons, B. J. Kirby, S. Roy, Z.-P. Li, I. V. Roshchin, S. K. Sinha, and I. K. Schuller, Phys. Rev. B **75**, 214412 (2007).

[52] E. Blackburn, C. Sanchez-Hanke, S. Roy, D. J. Smith, J.-I. Hong, K. T. Chan, A. E. Berkowitz, and S. K. Sinha, Phys. Rev. B **78**, 180408 (2008).

[53] S. Brück, G. Schütz, E. Goering, X. Ji, and K. M. Krishnan, Phys. Rev. Lett. **101**, 126402 (2008).

[54] C. Antoniak, J. Lindner, and M. Farle, Europhys. Lett. **70**(2), 250–256 (2005).